Springer

KSME

Journal of Mechanical Science and Technology 30 (9) (2016) 3929~3934
www.springerlink.com/content/1738-494x(Print)/1976-3824(Online)
DOI 10.1007/s12206-016-0804-3

Direct numerical simulation of 3D particle motion in an evaporating liquid film †

Hochan Hwang and Gihun Son*

Department of Mechanical Engineering, Sogang University, 35 Baekbeom-ro, Mapo-gu, Seoul 04107, Korea

(Manuscript Received October 21, 2015; Revised December 22, 2015; Accepted December 28, 2015)

Abstract

A direct numerical simulation method is developed for 3D particle motion in liquid film evaporation. The liquid-gas and fluid-solid interfaces are tracked by a sharp-interface Level-set (LS) method, which includes the effects of evaporation, contact line and solid particles. The LS method is validated through simulation of the interaction between two particles falling in a single-phase fluid. The LS based DNS method is applied to computation of the particle motion in liquid film evaporation to investigate the particle-interface and particle-particle interactions.

Keywords: Evaporation; Level- set method; Particle motion

1. Introduction

The particle motion in an evaporating liquid film is very important in fabrication of particulate microstructures [1]. Its predictive models were developed in several studies using the particle concentration [2-5], but the models have a limitation in analysis of the interaction between a particle and a fluid, a liquid-gas interface and other particles. Recently, Direct numerical simulation (DNS) methods were proposed for the particle interactions.

Glowinski et al. [6], Sharma and Patankar [7], and Apte et al. [8] performed DNS of particle-fluid and particle-particle interactions in a single-phase fluid employing a Fictitious domain (FD) method, where the particles were treated as the surrounding fluid region.

Mirzaii and Passandideh-Fard [9] combined the FD method and the Volume-of-fluid (VOF) method to investigate the particle-particle and particle-interface interactions. They assumed the particles as high-viscosity fluid and used a Piecewise linear interface calculation (PLIC) algorithm for reconstructing the interface. The PLIC VOF method is much complicated to implement in the region including three phases of liquid, gas and solid.

Fujita et al. [10] coupled an Immersed boundary (IB) method for a solid particle to a diffuse-interface Level-set (LS) method for a liquid-gas interface to compute the particle interactions in liquid evaporation. They assumed the vaporization rate constant instead of obtaining it from the conservation equations of energy and vapor concentration. Subsequently, Hwang and Son [11] applied a sharp-interface LS method to DNS of particle motion in microdroplet evaporation introducing two LS functions for the liquid-gas and fluid-solid interfaces.

In this study, we further extend the LS method to compute 3D particle motion in an evaporating liquid film and investigate the associated particle-interface and particle-particle interactions.

2. Numerical analysis

We employ the LS method developed in our previous studies [11-13] for droplet evaporation and particle motion. The gas is assumed as an ideal mixture of air and vapor whereas the liquid as a pure substance.

The liquid-gas interface is represented by the LS function ϕ, which is determined to be a signed distance from the interface: $\phi \le 0$ for gas phase and $\phi > 0$ for liquid phase. The fluid-solid interface of an immersed solid particle is tracked by another LS function ψ, which is calculated as a signed distance from the fluid-solid interface: $\psi \le 0$ for solid phase and $\psi > 0$ for fluid phase. A typical example of the LS contours for the case where a particle is partly immersed is plotted in Fig. 1.

In this work, assuming solid spheres as particles, ψ is expressed as

$$\psi(\mathbf{x},t) = \left|\mathbf{x} - \mathbf{x}_p(t)\right| - d_p / 2 \tag{1}$$

where $\mathbf{x}_p$ is the position vector of particle centroid and d_p

*Corresponding author. Tel.: +82 2 705 8641, Fax.: +82 2 712 0799
E-mail address: gihun@sogang.ac.kr
This paper was presented at the AJK2015-FED, Seoul, Korea, July 2015.
† Recommended by Guest Editor Gihun Son and Hyoung-Gwon Choi

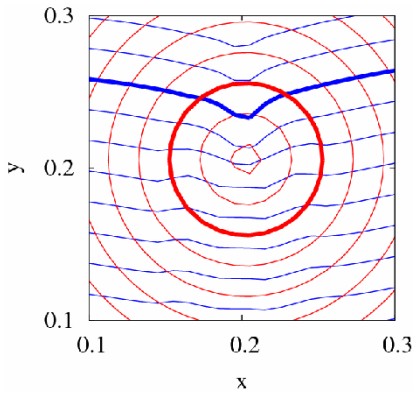

Fig. 1. A typical example of level-set (ϕ, ψ) contours for the case where a particle is partly immersed. The blue and red lines denote ϕ and ψ contours, respectively.

is the diameter of particles.

Assuming the solid domain is occupied by a high-viscosity non-evaporating fluid, the conservation equations of mass, momentum and energy for the liquid and gas phases and vapor mass fraction (Y_v) for the gas phase can be written as [11-13]

$$\nabla \cdot \mathbf{u} = \alpha_\psi \beta \dot{m} \mathbf{n} \cdot \nabla \alpha_\phi \tag{2}$$

$$\hat{\rho} \frac{\partial \mathbf{u}}{\partial t} = -[\nabla p + \alpha_\psi (\sigma\kappa - \beta \dot{m}^2) \nabla \alpha_\phi] + \nabla \cdot \hat{\mu} \nabla \mathbf{u} + \mathbf{f} \tag{3}$$

$$(\widehat{\rho c}) \frac{\partial T}{\partial t} = -(\widehat{\rho c}) \mathbf{u}_f \cdot \nabla T + \nabla \cdot \hat{\lambda} \nabla T \quad \text{if } \phi \neq 0 \text{ or } \psi \leq 0 \tag{4}$$

$$T = T_I \quad \text{if } \phi = 0 \text{ and } \psi > 0 \tag{5}$$

$$\frac{\partial Y_v}{\partial t} = -\mathbf{u}_g \cdot \nabla Y_v + \nabla \cdot \hat{D}_v \nabla Y_v \quad \text{if } \phi < 0 \text{ and } \psi > 0 \tag{6}$$

$$Y_v = Y_{v,I} \quad \text{if } \phi = 0 \text{ and } \psi > 0 \tag{7}$$

where

$$\beta = \rho_g^{-1} - \rho_l^{-1}$$
$$\alpha_\phi = 1 \text{ if } \phi > 0$$
$$\alpha_\phi = 0 \text{ if } \phi \leq 0$$
$$\alpha_\psi = 1 \text{ if } \psi > 0$$
$$\alpha_\psi = 0 \text{ if } \psi \leq 0$$
$$\mathbf{n} = \nabla\phi / |\nabla\phi|$$
$$\kappa = \nabla \cdot \mathbf{n}$$
$$\hat{\rho} = [\rho_g (1 - F_\phi) + \rho_l F_\phi] F_\psi + \rho_s (1 - F_\psi)$$
$$\hat{\mu}^{-1} = [\mu_g^{-1} (1 - F_\phi) + \mu_l^{-1} F_\phi] F_\psi + \mu_s^{-1} (1 - F_\psi)$$
$$(\widehat{\rho c}) = [(\rho c)_g (1 - \alpha_\phi) + (\rho c)_l \alpha_\phi] \alpha_\psi + (\rho c)_s (1 - \alpha_\psi)$$
$$\hat{\lambda}^{-1} = [\lambda_g^{-1} (1 - \alpha_\phi)(1 - F_\phi) + \lambda_l^{-1} \alpha_\phi F_\phi] F_\psi + \lambda_s^{-1} (1 - F_\psi)$$
$$\hat{D}_v^{-1} = D_v^{-1} (1 - F_\phi)$$
$$\mathbf{f} = -\hat{\rho} \mathbf{u}_f \cdot \nabla \mathbf{u}_f + \hat{\rho} g + \nabla \cdot \hat{\mu} (\nabla \mathbf{u}_f - \beta \dot{m} \mathbf{n} \nabla \alpha_\phi)^T . \tag{8}$$

Here, the subscript *f* denotes the gas phase (*g*) for $\phi \leq 0$ and the liquid phase (*l*) for $\phi > 0$. The effective properties $\hat{\rho}$, $\hat{\mu}$, $\hat{\lambda}$ and $\hat{D}_v$ are interpolated by using a fraction function F_ϕ [13]. The temperature T_I, the vapor fraction $Y_{v,I}$ and the evaporation mass flux $\dot{m}$ at the interface ($\phi = 0$) are simultaneously calculated from the following mass and energy balances and the thermodynamic relation

$$\dot{m} = \frac{\mathbf{n} \cdot \rho_g \hat{D}_v \nabla Y_v}{(1 - Y_{v,I})} = \frac{\mathbf{n} \cdot [(\hat{\lambda} \nabla T)_{\phi > 0} - (\hat{\lambda} \nabla T)_{\phi < 0}]}{h_{lg}} \tag{9}$$

$$Y_{v,I} = \frac{M_v p_{v,sat}(T_I)}{M_v p_{v,sat}(T_I) + M_a [p_\infty - p_{v,sat}(T_I)]} . \tag{10}$$

The LS function including $\phi = 0$ for the interface is advanced as

$$\frac{\partial \phi}{\partial t} = -\mathbf{U} \cdot \nabla \phi \quad \text{if } \psi > 0 \tag{11}$$

$$\frac{\partial \phi}{\partial \tau} = \cos\theta_s - \mathbf{n}_s \cdot \nabla \phi \quad \text{if } \psi \leq 0 \tag{12}$$

where the interface velocity $\mathbf{U}$ and the unit normal vector is $\mathbf{n}_s$ pointing into the solid domain are expressed as

$$\mathbf{U} = \mathbf{u}_l + \dot{m} \mathbf{n} / \rho_l \tag{13}$$

$$\mathbf{n}_s = -\nabla\psi / |\nabla\psi| . \tag{14}$$

The contact angle condition specified at contact line is implemented in the entire solid domain by using Eq. (12), which is iteratively solved as

$$\frac{\phi^{m+1} - \phi^m}{\Delta\tau} = \cos\theta_s - \mathbf{n}_s \cdot \nabla \phi^m \quad \text{if } \psi \leq 0 . \tag{15}$$

Here, the superscript *m* denotes the iteration step. The LS function is reinitialized as

$$\frac{\partial \phi}{\partial \tau} = \frac{\phi}{\sqrt{\phi^2 + h^2}} (1 - |\nabla\phi|) \quad \text{if } |\phi| \geq h/2 \tag{16}$$

where *h* is a grid spacing.

To impose the rigid body motion, the velocity inside the solid domain is modified as

$$\mathrm{u} = \mathrm{u}_p + \boldsymbol{\omega}_p \times (\mathbf{x} - \mathbf{x}_p) \tag{17}$$

where u_p and $\boldsymbol{\omega}_p$ of the particle centroid are determined from the following conservation condition of the linear and angular momenta in each particle domain [7],

$$\mathrm{u}_p = \frac{1}{V_p} \int \mathrm{u} \, dV_p \tag{18}$$

$$\boldsymbol{\omega}_p = \frac{\rho_p}{I_p}\int (\mathbf{x}-\mathbf{x}_p)\times \mathrm{u}\, dV_p \tag{19}$$

where V_p is the particle volume and I_p is the moment of inertia of the particle.

To treat particle-particle collision, a special numerical treatment reported by Diaz-Goano et al. [14] is used so that the particle should not overlap the other particle.

3. Results and discussion

3.1 Two-particle sedimentation a non-evaporating fluid

The LS formulation including the effect of particle-particle interaction is tested through a 3D computation of two particles falling in a single-phase fluid under gravity, whose numerical result was presented by Apte et al. [8]. The computational domain is chosen as a rectangular region of $0 \le x, z \le 1$ cm and $0 \le y \le 4$ cm including the two spherical particles whose centers are initially positioned at $\mathbf{x}_p = (0.5, 3.5, 0.5)$ cm and $\mathbf{x}_p = (0.5, 3.16, 0.5)$ cm. No-slip wall condition is imposed at the boundaries. We use the following properties of fluid and particle: $\rho_l = 10^3$ kg / m^3, $\mu_l = 10^{-3}$ Pa s, $\rho_s = 1.14\times10^3$ kg / m^3, $g = 9.8$ m / s^2 and $d_p = (1/6)$ cm. In the LS formulation, the solid region is treated as a high viscosity non-evaporating fluid of $\mu_s = 10^3 \mu_l$. The particles and fluid are initially stationary. The computation is conducted with a mesh size of $h = (1/64)$ cm and a time step of $\Delta t = 0.5$ ms. The numerical results for the particle-particle interaction are plotted in Figs. 2 and 3. As the particle velocities increase with gravity, vortex flows are induced around the particles and the upper particle falls faster in the wake region created by the lower particle. This results in a decrease in the distance between the two particles. The present prediction of the particle sedimentation positions and velocities in the vertical direction shows a good agreement with the numerical results of Apte et al. [8].

3.2 Particle motion in an evaporating liquid film

The LS method is applied to DNS of particle motion in an evaporating liquid film. The computational domain is chosen as a rectangular region of $|x, z| \le 3.2\,\mu$m and $0 \le y \le 6.4\,\mu$m. We use the slip condition at $|z| = 3.2\,\mu$m, the open boundary condition at $y = 6.4\,\mu$m and the no-slip condition at the side and bottom walls ($x = |3.2|\,\mu$m and $y = 0$)

$$\mathbf{u} = 0,\ T = T_w,\ \frac{\partial Y_v}{\partial x} = 0,\ \frac{\partial \phi}{\partial x} = \pm\cos\theta_{sw} \ \text{ at } \ x = \pm 3.2\,\mu\text{m} \tag{20}$$

$$\mathbf{u} = 0,\ T = T_w,\ \frac{\partial Y_v}{\partial y} = 0,\ \frac{\partial \phi}{\partial y} = -\cos\theta_{bw} \ \text{ at } \ y = 0 \tag{21}$$

where the contact angle θ_w formed on the contact line can vary dynamically between θ_a and θ_r, which was described in Refs. [12, 13, 15, 16].

We choose the following water and air properties:

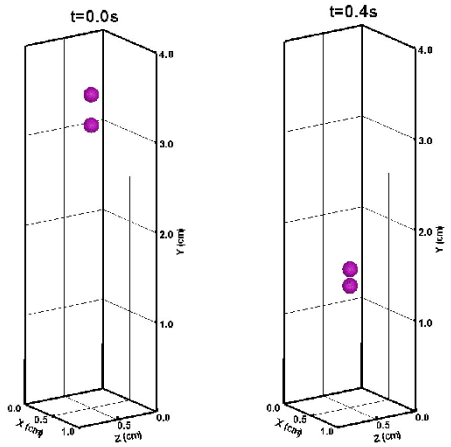

Fig. 2. 3D numerical results of two-particle sedimentation in a non-evaporating fluid.

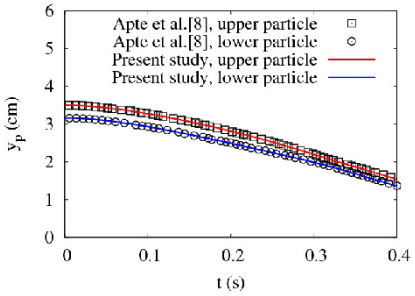

(a)

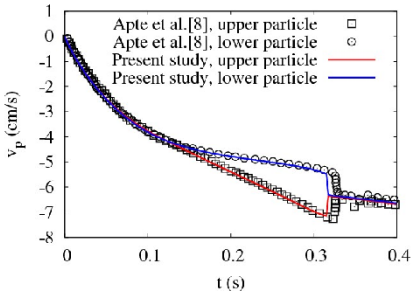

(b)

Fig. 3. 3D numerical results for two-particle sedimentation in a non-evaporating fluid: (a) Particle positions; (b) particle velocities in the vertical direction.

$\rho_l = 997$ kg / m^3, $\rho_g = 1.18$ kg / m^3, $\rho_s = 997$ kg / m^3,
$c_l = 4.18\times10^{-3}$ J / kgK, $c_g = 1.01\times10^{-3}$ J / kgK, $c_s = 318$ J / kgK,
$\mu_l = 8.91\times10^{-4}$ Pas, $\mu_g = 1.85\times10^{-5}$ Pas, $D_g = 2.6\times10^{-5}$ m^2 / s,
$\lambda_l = 0.595$ W / mK, $\lambda_g = 2.55\times10^{-2}$ W / mK, $\lambda_s = 31$ W / mK,
$\sigma = 7.2\times10^{-2}$ N / m and $\theta_s = 30°$.

The saturated-vapor pressure is evaluated as a function of temperature from the steam table [17].

We use the wall temperature as $T_w = 80°$C, the initial temperature as $T = 25°$C, the vapor concentration at the open boundary as $Y_v = 0$, the particle diameter as $d_p = 1\,\mu$m, the

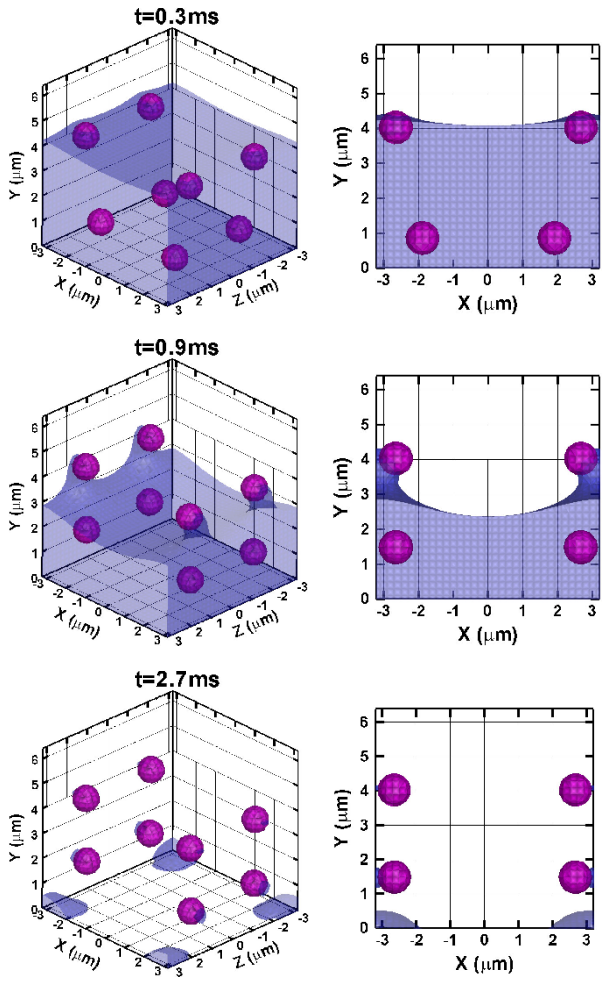

Fig. 4. Particle motion in liquid film evaporation with $\theta_{sw,r} = 90°$ and initial particle locations of $(\pm 2.4, 3.5, \pm 1.6)\,\mu$m and $(\pm 1.2, 0.8, \pm 1.6)\,\mu$m.

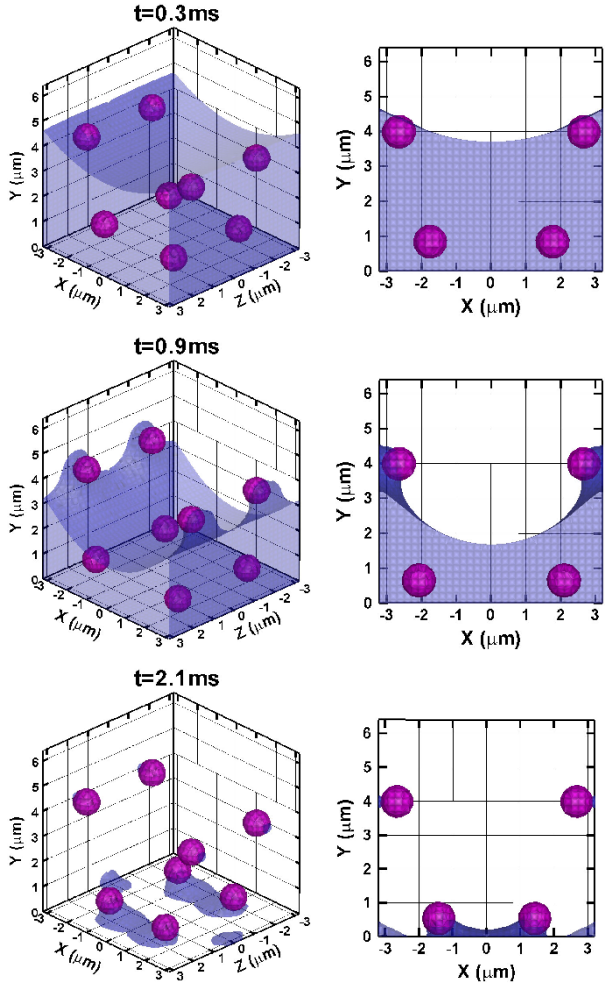

Fig. 5. Particle motion in liquid film evaporation with $\theta_{sw,r} = 60°$ and initial particle locations of $(\pm 2.4, 3.5, \pm 1.6)\,\mu$m and $(\pm 1.2, 0.8, \pm 1.6)\,\mu$m.

initial liquid film height as $y = 5\,\mu$m, the advancing contact angle as $\theta_a = 90°$, the receding contact angle at the side wall as $\theta_{sw,r} = 90°$ or $60°$, and the receding contact angle at the bottom wall as $\theta_{bw,r} = 30°$. Calculations are carried out with a uniform mesh of $h = 0.2\,\mu$m and a time step of $\Delta t = 5 \times 10^{-3}\,\mu$s.

Fig. 4 shows the particle motion with a contact angle of $\theta_{sw,r} = 90^o$ at the side walls and initial particle locations of $(\pm 2.4, 3.5, \pm 1.6)\,\mu$m and $(\pm 1.2, 0.8, \pm 1.6)\,\mu$m. The liquid-gas interface moves down as the liquid volume decreases with evaporation while the upper particles touch the side walls, as seen at t = 0.3 ms. Thereafter, the contact line near the touched upper particles is stuck on the side walls and then slips as the other part of contact line keeps moving down. This behavior of interface and upper particle induces a circulated flow in the liquid pool and causes the initially lower particles to rise up slightly and then to be deposited on the side walls.

When the side wall contact angle is reduced to $\theta_{sw,r} = 60^o$, the particle behavior is plotted in Fig. 5. As the liquid-gas interface is further deformed to have a concave shape with the decreased contact angle, the circulated flow becomes stronger and the lower particles are pushed down and then deposited on the bottom wall, as seen as t = 2.1 ms, but the upper particle deposition on the side walls occurs in the same way with the previous case of $\theta_{sw,r} = 90^o$. This indicates that the deposition pattern of the lower particles is affected by the contact angle at the side walls.

The effect of side wall receding angle $\theta_{sw,r}$ on the motion of lower particles is further investigated through the computations without the upper particles, as presented in Fig. 6. In the case of $\theta_{sw,r} = 90°$, the lower particles rise up and then touch the side walls, as seen in Fig. 4 including the upper particles. When $\theta_{sw,r}$ is decreased to $60°$ and the circulated flow becomes stronger, the lower particles move to the center line and then are pushed down to the bottom wall, as observed in Fig. 5 with the upper particles. This means that the motion of the lower particles is not sensitive to the upper particle motion as long as the upper particles are located near the side wall.

Fig. 7 shows the particle motion with $\theta_{sw,r} = 60°$ when the upper particles are at $(\pm 1.2, 3.5, \pm 1.6)\,\mu$m near the central

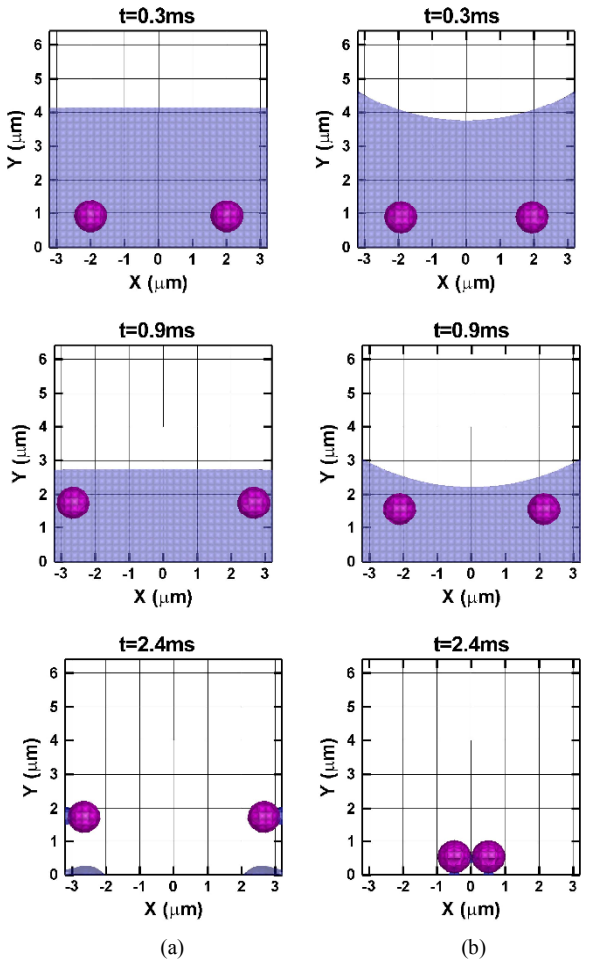

Fig. 6. Effect of side wall receding angle of $\theta_{sw,r}$ on the motion of lower particles at $(\pm 1.2, 0.8, \pm 1.6)\mu$m without including the upper particles: (a) $\theta_{sw,r} = 90°$; (b) $\theta_{sw,r} = 60°$.

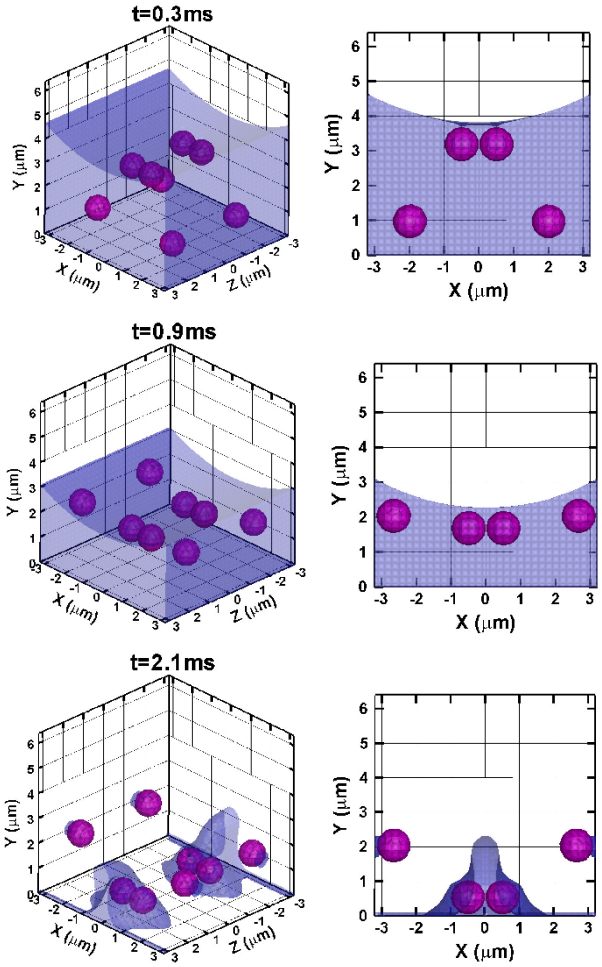

Fig. 7. Particle motion in liquid film evaporation with $\theta_{sw,r} = 60°$ and initial particle locations of $(\pm 1.2, 3.5, \pm 1.6)\mu$m and $(\pm 1.2, 0.8, \pm 1.6)\mu$m.

region. As the interface is deformed with evaporation, the upper particles move to the mid plane and then downwards with the interface. The circulated flow along with the upper particle pushes the lower particles outwards to the side wall, as seen at t = 0.9 ms. While the upper particles touch on the bottom wall, the lower particles are deposited on the side walls unlike the previous cases depicted in Figs. 5 and 6(b) where the upper particles are initially located near the side wall.

4. Conclusions

A Direct numerical simulation (DNS) method for the particle-fluid and particle-particle interactions was developed by introducing a Level-set (LS) function for tracking the solid region, which was treated as a high-viscosity fluid phase. The DNS method was validated through the 3D computation of two particles falling in a single-phase fluid whose numerical result was reported in the literature. The DNS method was extended for 3D particle motion in liquid film evaporation using two LS functions for tracking the liquid-gas and fluid-solid and interfaces. The DNS method was demonstrated to be applicable to investigate the particle-interface and particle-particle interactions in liquid evaporation.

Nomenclature

c	: Specific heat
d_p	: Particle diameter
D_v	: Diffusion coefficient of vapor in air
F	: Fraction function
g	: Gravity
h	: Grid spacing
h_{lg}	: Latent heat of vaporization
I_p	: Moment of inertia of a particle
$\dot{m}$	: Mass flux across the liquid-gas interface
M	: Molecular mass
$\mathbf{n}$	: Unit normal vector
p	: Pressure
t	: Time
T	: Temperature

u : Fluid velocity vector (*u, v, w*)
U : Interface velocity vector
V : Volume
x, y, z : Cartesian coordinates
x : Position vector (*x, y, z*)
Y_v : Vapor mass fraction

Greek symbols

α : Step function
θ_a : Advancing contact angle
θ_r : Receding contact angle
θ_s : Contact angle on a solid particle
κ : Interface curvature
λ : Thermal conductivity
μ : Dynamic viscosity
ρ : Density
σ : Surface tension coefficient
τ : Artificial time
ϕ : Distance function from the liquid-gas interface
ψ : Distance function from the fluid-solid interface
ω : Angular velocity

Subscripts

a : Air
bw : Bottom wall
f : Fluid
g : Gas
I : Interface
l : Liquid
p : Particle or particle centroid
s : Solid
sat : Saturation
sw : Side wall
v : Vapor
∞ : Ambient

Reference

[1] A. F. Routh, Drying of thin colloidal films, *Rep. Prog. Phys.,* 76 (2013) 046603.
[2] E. Widjaja and M. T. Harris, Particle deposition study during sessile drop evaporation, *AICHE*, 54 (2008) 2250-2260.
[3] R. Bhardwaj, X. Fang and D. Attinger, Pattern formation during the evaporation of a colloidal nanoliter drop: a numerical and experimental study, *New J. Phys.,* 11 (2009) 075020.
[4] K. L. Maki and S. Kumar, Fast evaporation of spreading droplets of colloidal suspensions, *Langmuir,* 27 (2011) 11347-11363.
[5] J. Lee and G. Son, A level-set method for analysis of particle motion in an evaporating microdroplet, *Numer. Heat Transfer B,* 67 (2015) 25-46.
[6] R. Glowinski, T. W. Pan, T. I. Hesla, D. D. Joseph and J. Periaux, A fictitious domain approach to the direct numerical simulation of incompressible viscous flow past moving rigid bodies: application to particulate flow, *J. Comput. Phys.*, 169 (2001) 363-426.
[7] N. Sharma and N. A. Patankar, A fast computation technique for the direct numerical simulation of rigid particulate flows, *J. Comput. Phys.*, 205 (2005) 439-457.
[8] S. V. Apte, M. Martin and N. A. Patankar, A numerical method for fully resolved simulation (FRS) of rigid particle-flow interactions in complex flows, *J. Comput. Phys.,* 228 (2009) 2712-2738.
[9] I. Mirzaii and M. Passandideh-Fard, Modeling free surface flows in presence of an arbitrary moving object, *Int. J. Multiphase Flow*, 39 (2012) 216-226.
[10] M. Fujita, O. Koike and Y. Yamaguchi, Direct simulation of drying colloidal suspension on substrate using immersed free surface model, *J. Comput. Phys.*, 281 (2015) 421-448.
[11] H. Hwang and G. Son, A level-set method for direct numerical simulation of particle motion in droplet evaporation, *Numer. Heat Transfer B,* 68 (2015) 479-494.
[12] G. Son, A level-set method for analysis of microdroplet evaporation on a heated surface, *J. Mech. Sci. Technol.,* 24 (2010) 991-997.
[13] G. Son, Numerical simulation of microdroplet impact and evaporation on a solid surface, *J. Heat Transfer,* 134 (2012) 101502.
[14] C. Diaz-Goano, P. D. Minev and K. Nandakumar, A fictitious domain/finite element method for particulate flows, *J. Comput. Phys*, 192 (2003) 105-123.
[15] J. Fukai, Y. Shiiba, T. Yamamoto, O. Miyatake, O. Poulikakos, C. M. Megaridis and Z. Zhao, Wetting effects on the spreading of a liquid droplet colliding with a flat surface, *Phys. Fluids,* 7 (1995) 236-247.
[16] H. Ban and G. Son, Numerical simulation of droplet evaporation between two circular plates, *J. Mech. Sci. Technol.,* 29 (2015) 2401-2407.
[17] F. L. Jr. Thomas and E. L. Peter, *Steam and Gas Tables with Computer Equations*, Academic Press (1984).

Hochan Hwang received his B.S. degree in Mechanical Engineering from Sogang University in 2013. He is currently a graduate student of Mechanical Engineering at Sogang University, Korea. Mr. Hwang's research interests are in the area of multiphase flow and heat transfer.

Gihun Son received his B.S. and M.S. degrees in Mechanical Engineering from Seoul National University in 1986 and 1988, respectively, and his Ph.D. degree in Mechanical Engineering from UCLA in 1996. Dr. Son is currently a Professor of Mechanical Engineering at Sogang University, Korea. His research interests are in the areas of heat transfer, multiphase flow and power plant.